Vapor-liquid equilibria and diffusion coefficients of difluoromethane, 1,1,1,2-tetrafluoroethane and 2,3,3,3-tetrafluoropropene in low-viscosity ionic liquids

Authors:

Salvador Asensio-Delgado, Fernando Pardo, Gabriel Zarca*, Ane Urtiaga

Department of Chemical and Biomolecular Engineering, Universidad de Cantabria,

Av. Los Castros 46, Santander 39005, Spain.

*Corresponding author e-mail address: zarcag@unican.es

Abstract

The phase-down of hydrofluorocarbons (HFCs) established by the Kigali Amendment to the Montreal Protocol is leading to the formulation and commercialization of new refrigerant blends containing hydrofluoroolefins (HFOs), such as 2,3,3,3-tetrafluoropropene (R1234yf), and HFCs with moderate global warming potential, namely, difluoromethane (R32) and 1,1,1,2-tetrafluoroethane (R134a). Moreover, the recycling of refrigerants is attracting attention as a means to reduce the amount of new HFCs produced and their release to the environment. To that end, the use of ionic liquids has been proposed as entrainers to separate refrigerants with close-boiling points or azeotropic blends. Thus, the vapor-liquid equilibria and diffusion coefficients of the refrigerant-ionic liquid pairs formed by R32 + $[C_2mim][BF_4]$, R134a + $[C_2mim][BF_4]$, R134a+ $[C_2mim][OTf]$, R1234yf + $[C_2mim][OTf]$ and R1234yf + $[C_2mim][Tf_2N]$ are studied using an isochoric saturation method at temperatures ranging from 283.15 to 323.15 K and pressures up to 0.9 MPa. In addition, the solubility behavior is successfully modeled using the non-random two-liquid activity coefficient method, and the Henry's law constants at infinite dilution, solvation energies and infinite dilution activity coefficients are calculated.

1. Introduction

Hydrofluorocarbons (HFCs) are fluorinated gases widely used in refrigeration and air conditioning (RAC) as substitutes for the ozone-depleting substances that were phased out under the Montreal Protocol (MP).[1,2] Despite their zero ozone depletion potential (ODP), HFCs still exhibit high global warming potential (GWP), which makes them environmentally concerning greenhouse gases[3] to be phased out under the Kigali Amendment to the MP. In contrast, hydrofluoroolefins (HFOs) have been proposed as a new generation of refrigerants because of their zero ODP, low GWP, and short atmospheric lifetime.[4] One of the most common HFOs is 2,3,3,3-tetrafluoropropene (R1234yf, GWP = 4), which is being currently used in pure form in mobile air conditioning systems by the automotive sector. However, HFOs are mildly flammable (ASHRAE category A2L) and their use is constraint to a limited set of temperatures, thus affecting the refrigeration efficiency in refrigerators and freezers of commercial use when used as pure compounds.[5–7] For these reasons, HFOs are usually blended with HFCs such as difluoromethane (R32, GWP = 675) and 1,1,1,2-tetrafluoroethane (R134a, GWP = 1430), which are very well-known refrigerants with a strong penetration in the RAC market. These HFC/HFO blends (e.g., R513A, R454C, R449A) are being commercialized as environmentally friendly drop-in replacements of typical HFC-only mixtures (e.g., R410A, R404A, R407 series).

Ionic liquids (ILs) are a family of compounds that has attracted attention in several fields because of their interesting properties, namely, extremely low vapor pressure, chemical and thermal stability, wide liquid temperature range or non-flammability, among others.[8–10] The use of ILs as entrainers has been proposed to allow for the separation of azeotropic or close-boiling point blends of refrigerant gases,[10–24] and as working fluids in absorption refrigeration systems.[25–34] The efficient separation of refrigerant blends would promote a more circular economy in the RAC sector, whereby HFCs and HFOs recovered from end-of-life equipment are used to formulate novel low GWP blends.[35] In this sense, ILs provide several benefits over conventional

molecular solvents in the design of separation processes because solvent evaporation is avoided, and they are not flammable nor corrosive and do not release toxic vapors.[36] Furthermore, the separation of some HFC/HFO refrigerant mixtures by conventional methods is challenging because these blends typically have very small temperature glide, i.e., small difference between the refrigerant blend dew point and bubble point at constant pressure (e.g., system R32 + R1234yf) or present azeotropic behavior (e.g., system R134a + R1234yf),[37–39] which makes necessary the use of a mass separation agent to improve the purification process.

Thus, this work focuses on increasing current knowledge on the ability of ILs to perform the separation of new HFC/HFO refrigerant blends. We are particularly interested in examining the absorption of common HFCs and HFOs into low-viscosity ILs. The interest in low-viscosity ILs arises as a means to overcome scale-up problems associated to low mass transfer rates and high pumping costs of highly viscous ILs.[36,40] Moreover, the absorption process in ILs is reported to be kinetically controlled so that using low-viscosity ILs would enhance gas diffusion coefficients and, consequently, lead to higher recoveries and more energy-efficient separations.[41] Thus, we present the experimental gas solubility and diffusion coefficients of refrigerants R32, R134a and R1234yf in 1-ethyl-3-methylimidazolium tetrafluoroborate ($[C_2mim][BF_4]$), 1-ethyl-3-methylimidazolium trifluoromethanesulfonate ($[C_2mim][OTf]$) and 1-ethyl-3-methylimidazolium bis(trifluoromethylsulfonyl)imide ($[C_2mim][Tf_2N]$) for the binary systems that have not been previously reported in the literature, at temperatures ranging from 283.15 to 323.15 K and pressures up to 0.9 MPa. In addition, the solubility behavior is modeled using the non-random two-liquid activity coefficient model (NRTL).

2. Experimental section

2.1. Materials.

R32 (99.9%) was purchased from Coproven Climatización (Gas Servei licensed supplier, Spain). R134a (99.8%) and R1234yf (99.9%) were supplied by Carburos Metálicos (Air Products group, Spain). The ILs [C_2mim][BF_4], [C_2mim][OTf] and [C_2mim][Tf_2N] were purchased from Sigma-Aldrich. Before use, the three ILs were vacuum dried at 333 K for 24 h and their water content was measured using the Karl Fischer titration. The purity of all compounds and the viscosity and water content of ILs are specified in Table 1.

Table 1. Chemical samples used in this work

Chemical	CAS No.	Supplier	Fraction purity	μ/mPa·s	Purification method	Water content (ppm)
[C_2mim][BF_4]	143314-16-3	Sigma-Aldrich, Inc.	>98 wt %	32.31[42]	Vacuum drying	15
[C_2mim][OTf]	145022-44-2	Sigma-Aldrich, Inc.	>98 wt %	35.98[43]	Vacuum drying	10
[C_2mim][Tf_2N]	174899-82-2	Sigma-Aldrich, Inc.	>98 wt %	26.9[44]	Vacuum drying	10
R32	75-10-5	Gas Servei, S.A.	>99.9 vol %			
R134a	811-97-2	Air Products and Chemicals, Inc.	>99.8 vol %			
R1234yf	754-12-1	Air Products and Chemicals, Inc.	>99.9 vol %			

2.2. Experimental apparatus and procedure.

An isochoric saturation method was used to measure the absorption of gases in the selected ILs. The experimental system, described in detail in previous works,[8,9,36] consists of an absorption chamber and a storage cylinder connected by a valve. The absorption chamber is a jacketed stirred tank reactor (Buchi, model Picoclave, 170 mL), equipped with a pressure transducer (Aplisens, model PCE-28, ±0.001 bar) and a Pt-100 temperature sensor, connected to a cryothermostatic bath (Julabo, model F25-ME, ±0.01 K). The storage cylinder (140 mL) is equipped with an absolute digital manometer (Keller, model Leo 2, ±0.001 bar). The absorption chamber was loaded with ~35 g (±0.0001 g) of the vacuum dried IL. The difference between the total available volume and loaded IL volume is large enough to ensure that the measurements are independent of IL volumetric expansion as will be shown by the validation experiments in

Figure 1. Before each experiment, the IL was degassed at 333 K for a minimum of 6 h. This experimental system allows for the determination of both solubility and diffusivity in a single experiment. First, the temperature and pressure of the gas-filled storage cylinder were recorded. Then, the valve connecting both sections was opened and the absorption process was allowed to proceed spontaneously for the first 20 minutes for diffusivity measurements.[45] After that, the stirrer was set to 500 rpm and gas absorption proceeded until the system reached equilibrium conditions, this is, when pressure remained constant for more than 20 minutes.

2.3. Solubility measurement

Solubility is derived from temperature and pressure data as follows. The molar fraction of refrigerant gas dissolved in the IL is defined as:

$$x = \frac{n_{abs}}{n_l + n_{abs}} \quad (1)$$

where n_l are moles of IL and n_{abs} are the total dissolved moles of refrigerant. The isochoric saturation method was applied in several steps so that n_{abs} is calculated from the amount of gas dissolved in each step, n_i, plus the amount dissolved in the previous k steps:

$$n_{abs} = n_i + \sum_{k=1}^{i-1} n_k \quad (2)$$

where n_i is calculated as the difference between the initial and final moles in the vapor phase as follows:

$$n_i = \rho_{(i,s)} \cdot V_s + \rho_{(i-1,c)} \cdot (V_c - V_l) - \rho_{(i,eq)} \cdot (V_s + V_c - V_l) \quad (3)$$

In Eq. (3), V_s, V_c and V_l are the storage cylinder, sorption chamber and loaded IL volumes (L), respectively, and $\rho_{i,s}$, $\rho_{i-1,c}$ and $\rho_{i,eq}$ are the gas molar densities (mol·L^{-1}) in the storage cylinder, the sorption chamber and at equilibrium conditions, respectively. Molar densities were

calculated from pressure and temperature data using the cubic Peng-Robinson equation of state to account for deviations from ideal behavior.[13,18,19]

The uncertainty in molar fraction values was calculated using the quadratic propagation of errors:

$$u(x) = \sqrt{\left(\frac{\partial x}{\partial n_{abs}}\right)^2 \cdot u(n_{abs})^2 + \left(\frac{\partial x}{\partial n_l}\right)^2 \cdot u(n_l)^2} \quad (4)$$

where u is standard uncertainty. The uncertainty in n_l is derived from the mass of IL, and the uncertainty in n_{abs} is:

$$u(n_{abs}) = \sqrt{\left(\frac{\partial n_{abs}}{\partial n_i}\right)^2 \cdot u(n_i)^2 + \sum_k \left(\frac{\partial n_{abs}}{\partial n_k}\right)^2 \cdot u(n_k)^2} \quad (5)$$

The uncertainty in dissolved moles in each step, $u(n_i)$, is calculated following the same principia from the uncertainty in each of the variables of Eq. (3).

2.4. Diffusivity calculation

Gas diffusion coefficients in the ILs at infinite dilution were calculated using the semi-infinite volume model, derived from the expression of Fickian diffusion:[45,46]

$$\frac{\partial C}{\partial t} = D\frac{\partial^2 C}{\partial y^2} \quad (6)$$

Here, C expresses the concentration of gas in the solution (mol·m^{-3}), t is time (s), D is diffusivity (m^2·s^{-1}) and y is the depth into the IL (m). Integration of Eq. (6) leads to the accumulated dissolved moles per unit area M_t from which diffusion coefficients are obtained:

$$M_t = \int_0^t \left(D\left(\frac{\partial C}{\partial y}\right)_{y=0}\right) dt = \sqrt{D}\left(2C_{y=t=0}\sqrt{\frac{t}{\pi}} - \frac{1}{2}mt\sqrt{\pi}\right) = \sqrt{D}\varepsilon \quad (7)$$

where $C_{y=t=0}$ is the initial concentration of gas in the surface and m is a mass transfer coefficient expressed in mol·m^{-3}·s$^{-1/2}$, both of them calculated according to:

$$C_{y=0} = C_{y=t=0} + m\sqrt{t} \tag{8}$$

with $C_{y=0}$ being the surface concentration defined as:[47]

$$C_{y=0} = \frac{\rho_{IL}}{M_{IL} \cdot \left(\frac{k_H}{f} - 1\right)} \tag{9}$$

In Eq. (9), ρ_{IL} and M_{IL} are the IL density (kg·m^{-3}) and molar mass (kg·mol^{-1}), respectively, and k_H is the Henry's law constant (MPa) calculated from solubility data:

$$k_H(T) = \lim_{x \to 0} \frac{f(P,T)}{x} \tag{10}$$

where f is the refrigerant fugacity (MPa) calculated using the Peng-Robinson equation of state. As Henry's law constants are defined at infinite dilution, Eq. (10) can be simplified to:[10,23]

$$k_H \approx \left(\frac{df}{dx}\right)_{x=0} \tag{11}$$

Thus, diffusivity calculation involves three least squares adjustments in Eqs. (7, 8, and 11) to determine the regression parameters D, m, $C_{y=t=0}$, and k_H. The uncertainties in these parameters was derived by rigorous statistical treatment of least squares adjustment to account for the uncertainities present in both the independent and dependent variables.[48]

3. Results and discussion

To validate the reliability and accuracy of our experimental system, the solubility of R1234yf in [C_2mim][BF_4] at 303.15 K, and R32 in [C_2mim][OTf] at 298.15 K was measured and compared with available data. Table 2 presents the results of the validation experiments and Figure 1 shows the excellent agreement with published data.[25,34]

Table 2. Mole-fraction solubility of R1234yf in [C_2mim][BF_4] and R32 in [C_2mim][OTf]

R1234yf + [C_2mim][BF_4]				R32 + [C_2mim][OTf]			
T/K	p/MPa	x	$u(x)$	T/K	p/MPa	x	$u(x)$
303.15	0.0607	0.0038	0.0002	298.15	0.0492	0.0296	0.0004
303.15	0.1411	0.0087	0.0003	298.15	0.0561	0.0336	0.0004
303.15	0.2323	0.0147	0.0004	298.15	0.1729	0.1007	0.0008
303.15	0.3263	0.0207	0.0006	298.15	0.2522	0.1481	0.0010
303.15	0.4223	0.0277	0.0009	298.15	0.3015	0.1679	0.0012
				298.15	0.4404	0.2469	0.0014

Standard uncertainties are $u(T)$ = 0.01 K and $u(p)$ = 0.001 bar. The standard uncertainties for molar fraction $u(x)$ are given in the table.

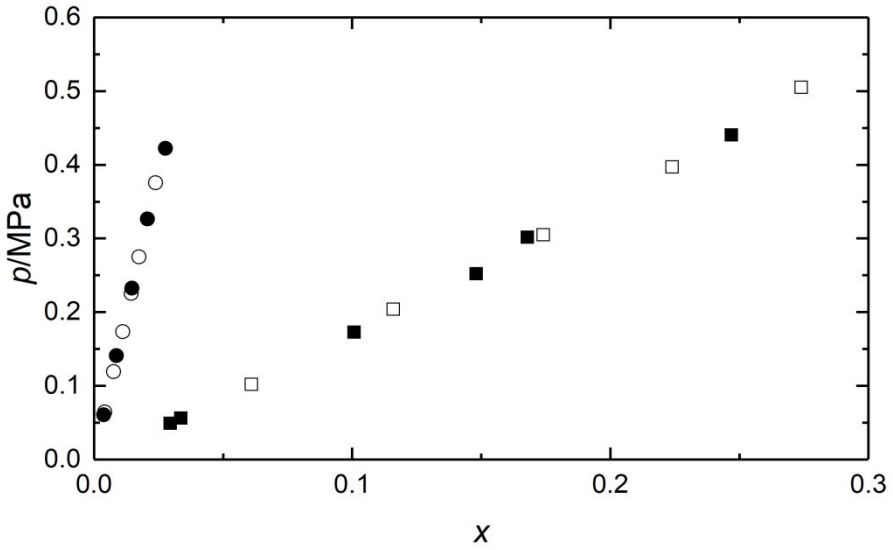

Figure 1. Solubility of refrigerant gases in ILs and comparison with literature data: system R1234yf + [C_2mim][BF_4] (●□), and system R32 + [C_2mim][OTf] (■). Hollow symbols are the literature data.[25,34]

The experimental data for the solubility of R32 and R134a in [C_2mim][BF_4], R134a and R1234yf in [C_2mim][OTf] and R1234yf in [C_2mim][Tf_2N] determined at temperatures between 283.15 and 323.15 K and pressures up to 0.9 MPa, are presented in Tables 3-7. In addition, Figures 2-6 show the experimental and calculated solubility isotherms for each of the refrigerant-IL pairs. As expected, the molar fraction of gas absorbed in the IL increases when temperature decreases and pressure increases.

Table 3. Mole-fraction solubility of R32 in $[C_2mim][BF_4]$

T/K	p/MPa	x	$u(x)$
283.15	0.0379	0.0260	0.0003
283.15	0.2510	0.1837	0.0013
283.15	0.3993	0.2869	0.0013
283.15	0.5031	0.3573	0.0014
283.15	0.5883	0.4155	0.0017
283.15	0.6549	0.4600	0.0020
283.15	0.7079	0.4962	0.0025
283.15	0.7509	0.5245	0.0031
293.15	0.0369	0.0212	0.0002
293.15	0.1769	0.1012	0.0008
293.15	0.3770	0.2099	0.0012
293.15	0.5156	0.2817	0.0013
293.15	0.6391	0.3443	0.0015
293.15	0.7524	0.3993	0.0018
293.15	0.8753	0.4582	0.0021
303.15	0.0459	0.0164	0.0002
303.15	0.2353	0.0961	0.0009
303.15	0.4500	0.1831	0.0012
303.15	0.6267	0.2499	0.0013
303.15	0.7504	0.2950	0.0016
303.15	0.8305	0.3262	0.0021
313.15	0.0482	0.0132	0.0002
313.15	0.1367	0.0409	0.0004
313.15	0.2502	0.0767	0.0006
313.15	0.4126	0.1262	0.0009
313.15	0.6648	0.1972	0.0013
313.15	0.8307	0.2423	0.0015
323.15	0.0552	0.0140	0.0002
323.15	0.2468	0.0617	0.0007
323.15	0.4939	0.1162	0.0010
323.15	0.6768	0.1551	0.0013
323.15	0.8639	0.1926	0.0016

Standard uncertainties are $u(T)$ = 0.01 K and $u(p)$ = 0.001 bar. The standard uncertainties for molar fraction, $u(x)$, are given in the table.

Table 4. Mole-fraction solubility of R134a in $[C_2mim][BF_4]$

T/K	*p*/MPa	*x*	*u*(*x*)
283.15	0.0374	0.0213	0.0002
283.15	0.1261	0.0888	0.0007
283.15	0.1994	0.1538	0.0008
283.15	0.2517	0.2073	0.0010
283.15	0.2899	0.2519	0.0012
283.15	0.3182	0.2885	0.0016
283.15	0.3400	0.3204	0.0020
283.15	0.3567	0.3473	0.0026
283.15	0.3697	0.3713	0.0034
283.15	0.3806	0.3915	0.0046
283.15	0.3890	0.4096	0.0061
283.15	0.3956	0.4266	0.0081
293.15	0.0430	0.0185	0.0002
293.15	0.1511	0.0761	0.0006
293.15	0.2439	0.1323	0.0008
293.15	0.3083	0.1750	0.0010
293.15	0.3525	0.2076	0.0013
293.15	0.3866	0.2352	0.0017
303.15	0.0473	0.0168	0.0002
303.15	0.1574	0.0583	0.0005
303.15	0.2685	0.1029	0.0007
303.15	0.3402	0.1343	0.0009
303.15	0.3952	0.1607	0.0012
303.15	0.4335	0.1788	0.0016
313.15	0.0520	0.0127	0.0002
313.15	0.1800	0.0462	0.0005
313.15	0.2905	0.0770	0.0007
313.15	0.3639	0.0988	0.0009
313.15	0.4161	0.1139	0.0012
313.15	0.4496	0.1245	0.0016
323.15	0.0520	0.0104	0.0002
323.15	0.1856	0.0361	0.0005
323.15	0.3257	0.0634	0.0007
323.15	0.4084	0.0805	0.0009
323.15	0.4590	0.0918	0.0012
323.15	0.4946	0.0986	0.0016

Standard uncertainties are $u(T)$ = 0.01 K and $u(p)$ = 0.001 bar. The standard uncertainties for molar fraction, $u(x)$, are given in the table.

Table 5. Mole-fraction solubility of R134a in [C_2mim][OTf]

T/K	*p*/MPa	*x*	*u*(*x*)
283.15	0.0308	0.0381	0.0004
283.15	0.0902	0.1151	0.0007
283.15	0.1639	0.2133	0.0010
283.15	0.2149	0.2842	0.0011
283.15	0.2522	0.3392	0.0013
283.15	0.2804	0.3833	0.0016
283.15	0.3027	0.4208	0.0020
293.15	0.0347	0.0298	0.0003
293.15	0.1018	0.0910	0.0006
293.15	0.1921	0.1747	0.0009
293.15	0.2557	0.2353	0.0011
293.15	0.3029	0.2818	0.0013
293.15	0.3369	0.3176	0.0017
293.15	0.3653	0.3483	0.0022
303.15	0.0396	0.0256	0.0003
303.15	0.1109	0.0720	0.0006
303.15	0.2178	0.1403	0.0009
303.15	0.2922	0.1891	0.0010
303.15	0.3457	0.2254	0.0013
303.15	0.3828	0.2513	0.0017
313.15	0.0422	0.0193	0.0003
313.15	0.1247	0.0574	0.0005
313.15	0.2396	0.1096	0.0008
313.15	0.3137	0.1440	0.0010
313.15	0.3674	0.1691	0.0013
313.15	0.4049	0.1869	0.0018
323.15	0.0513	0.0185	0.0003
323.15	0.1392	0.0500	0.0005
323.15	0.2662	0.0942	0.0008
323.15	0.3583	0.1257	0.0010
323.15	0.4216	0.1475	0.0013

Standard uncertainties are $u(T)$ = 0.01 K and $u(p)$ = 0.001 bar. The standard uncertainties for molar fraction, $u(x)$, are given in the table.

Table 6. Mole-fraction solubility of R1234yf in [C_2mim][OTf]

T/K	p/MPa	x	$u(x)$
283.15	0.0511	0.0163	0.0003
283.15	0.1430	0.0471	0.0006
283.15	0.2804	0.0972	0.0009
283.15	0.3731	0.1333	0.0011
283.15	0.4298	0.1577	0.0015
293.15	0.0550	0.0129	0.0003
293.15	0.1520	0.0357	0.0005
293.15	0.2898	0.0699	0.0009
293.15	0.3846	0.0961	0.0011
293.15	0.4481	0.1115	0.0014
303.15	0.0579	0.0103	0.0003
303.15	0.1633	0.0284	0.0005
303.15	0.3039	0.0536	0.0008
303.15	0.4188	0.0718	0.0011
303.15	0.4825	0.0839	0.0014
313.15	0.0609	0.0078	0.0003
313.15	0.1665	0.0211	0.0005
313.15	0.2927	0.0348	0.0007
313.15	0.4127	0.0459	0.0010
313.15	0.4801	0.0535	0.0013
323.15	0.0641	0.0051	0.0002
323.15	0.1756	0.0139	0.0005
323.15	0.3441	0.0240	0.0008
323.15	0.4319	0.0296	0.0010
323.15	0.4810	0.0344	0.0014

Standard uncertainties are $u(T)$ = 0.01 K and $u(p)$ = 0.001 bar. The standard uncertainties for molar fraction, $u(x)$, are given in the table.

Table 7. Mole-fraction solubility of R1234yf in $[C_2mim][Tf_2N]$

T/K	p/MPa	x	$u(x)$
283.15	0.1368	0.0985	0.0009
283.15	0.2644	0.2009	0.0013
283.15	0.3467	0.2725	0.0014
283.15	0.3983	0.3222	0.0017
283.15	0.4335	0.3602	0.0021
293.15	0.0499	0.0241	0.0004
293.15	0.1491	0.0758	0.0008
293.15	0.2860	0.1503	0.0012
293.15	0.3698	0.1978	0.0014
293.15	0.4257	0.2311	0.0018
303.15	0.0550	0.0194	0.0004
303.15	0.1555	0.0581	0.0008
303.15	0.2912	0.1099	0.0011
303.15	0.3853	0.1464	0.0014
303.15	0.4462	0.1710	0.0018
313.15	0.0566	0.0162	0.0004
313.15	0.1700	0.0497	0.0008
313.15	0.2816	0.0817	0.0010
313.15	0.4026	0.1148	0.0014
313.15	0.4796	0.1366	0.0018
323.15	0.0581	0.0134	0.0004
323.15	0.1605	0.0359	0.0007
323.15	0.3259	0.0702	0.0011
323.15	0.4213	0.0901	0.0014
323.15	0.4767	0.0996	0.0019

Standard uncertainties are $u(T)$ = 0.01 K and $u(p)$ = 0.001 bar. The standard uncertainties for molar fraction, $u(x)$, are given in the table.

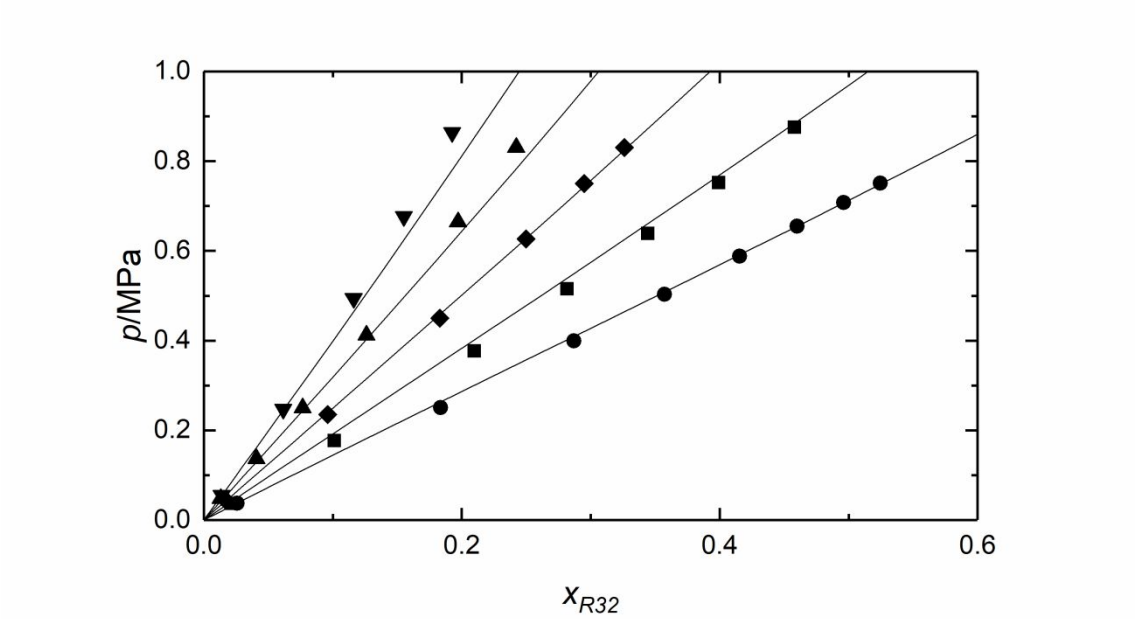

Figure 2. Solubility of R32 in $[C_2mim][BF_4]$ at various temperatures: 283.15 (●), 293.15 (■), 303.15 (♦), 313.15 (▲) and 323.15 K (▼). Solid lines represent NRTL model calculations.

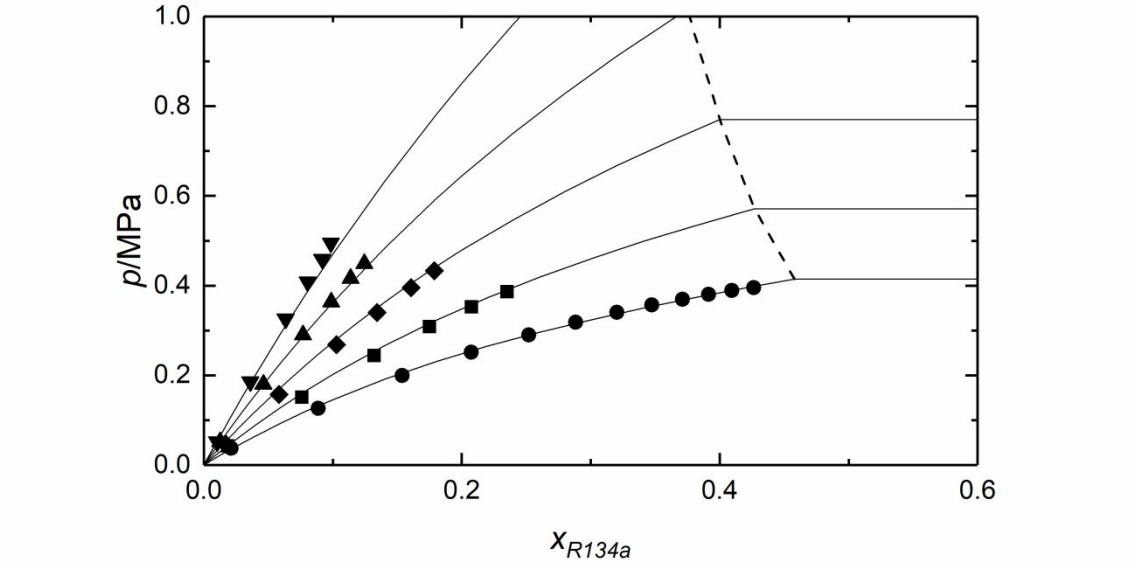

Figure 3. Solubility of R134a in $[C_2mim][BF_4]$ at various temperatures: 283.15 (●), 293.15 (■), 303.15 (♦), 313.15 (▲) and 323.15 K (▼). Solid lines represent NRTL model calculations and dashed lines represent the NRTL VLLE prediction.

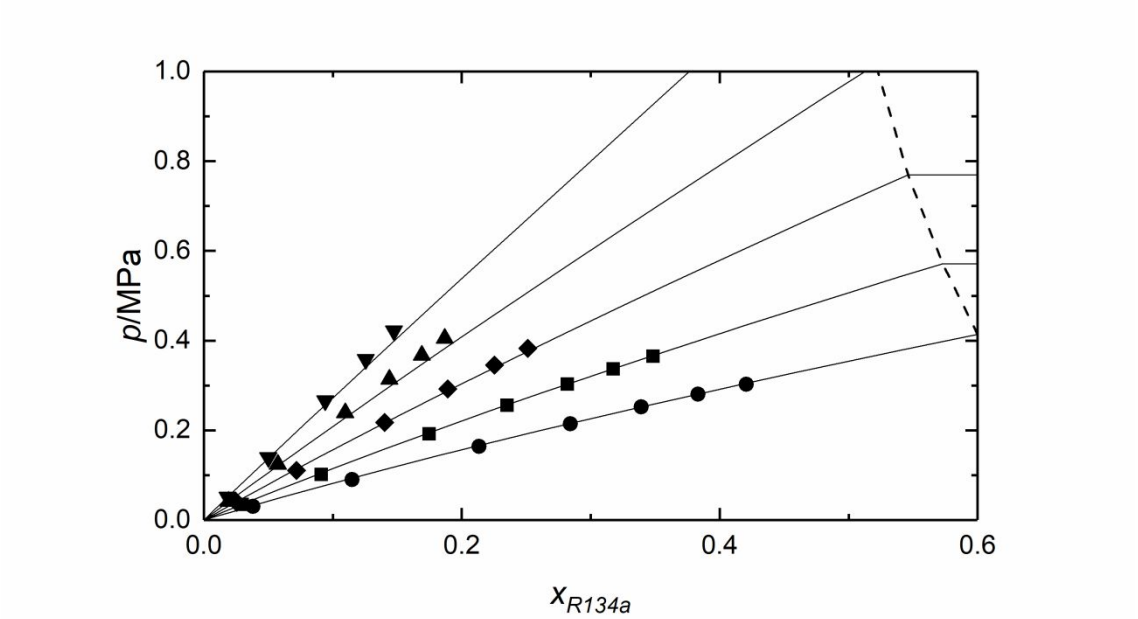

Figure 4. Solubility of R134a in [C_2mim][OTf] at various temperatures: 283.15 (●), 293.15 (■), 303.15 (♦), 313.15 (▲) and 323.15 K (▼). Solid lines represent NRTL model calculations and dashed lines represent the NRTL VLLE prediction.

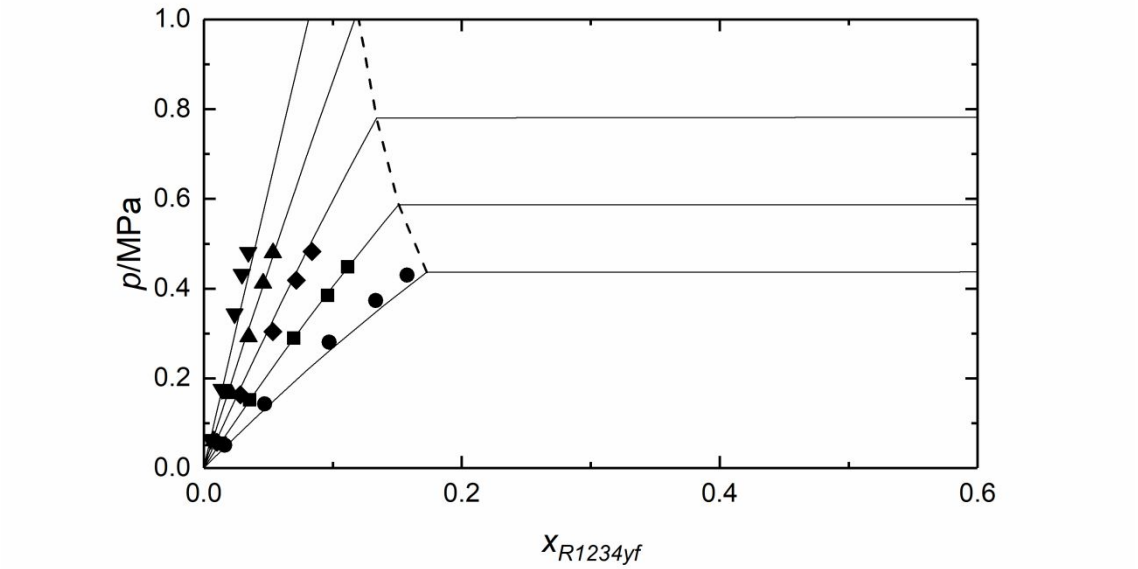

Figure 5. Solubility of R1234yf in [C_2mim][OTf] at various temperatures: 283.15 (●), 293.15 (■), 303.15 (♦), 313.15 (▲) and 323.15 K (▼). Solid lines represent NRTL model calculations and dashed lines represent the NRTL VLLE prediction.

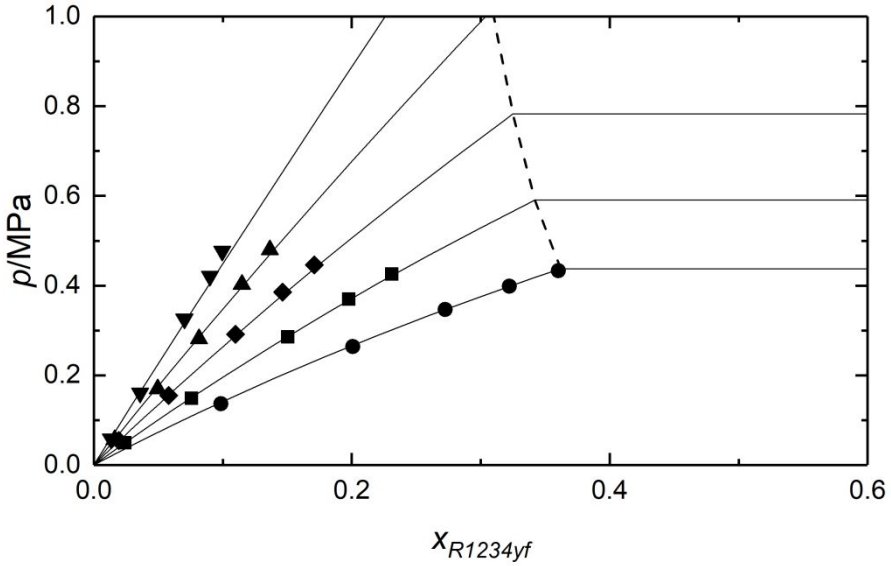

Figure 6. Solubility of R1234yf in [C_2mim][Tf_2N] at various temperatures: 283.15 (●), 293.15 (■), 303.15 (♦), 313.15 (▲) and 323.15 K (▼). Solid lines represent NRTL model calculations and dashed lines represent the NRTL VLLE prediction.

Experimental solubility data were modeled using the non-random two-liquid model (NRTL), an activity-coefficient model widely applied to this type of systems.[10,34,49] The vapor-liquid equilibria for each component of a mixture can be described by:

$$y_i p \Phi_i = x_i \gamma_i p_i^S \ (i \in \mathbb{Z}\ [1,N]) \tag{12}$$

where y_i and x_i are molar fractions of the i species in vapor and liquid phases, respectively, and γ_i and p_i^S are the activity coefficient and vapor pressure, respectively.

The correction factor, Φ_i, is calculated as:

$$\Phi_i = \exp\left[\frac{\left(B_i - V_i^L\right)\left(p - p_i^S\right)}{RT}\right] \tag{13}$$

where R is the ideal gas constant, B_i is the second virial coefficient and V_i^L is the saturated liquid molar volume. p_i^S, B_i and V_i^L were calculated using CoolProp 6.3.0 software.[50] CoolProp is a powerful tool that calculates physical properties of refrigerant gases from multiparameter

Helmholtz-energy-explicit-type equations of state specifically developed for each individual compound.[50–53] Combination of Eqs. (12) and (13) leads to the following expression of the activity coefficients:

$$\gamma_1 = \frac{p}{x_1 p_1^S} \exp\left[\frac{\left(B_1 - V_1^L\right)\left(p - p_1^S\right)}{RT}\right] \tag{14}$$

In addition, the following expression is used to calculated the activity coefficients according to the NRTL model:

$$\ln \gamma_1 = x_2^2 \left[\tau_{21}\left(\frac{G_{21}}{x_1 + x_2 G_{21}}\right)^2 + \frac{\tau_{12} G_{12}}{\left(x_2 + x_1 G_{12}\right)^2}\right] \tag{15}$$

where

$$G_{12} = \exp\left(-\alpha\tau_{12}\right), \quad G_{21} = \exp\left(-\alpha\tau_{21}\right) \tag{16}$$

$$\tau_{12} = \tau_{12}^0 + \frac{\tau_{12}^1}{T}, \quad \tau_{21} = \tau_{21}^0 + \frac{\tau_{21}^1}{T} \tag{17}$$

The tendency of two species to distribute in an organized way is characterized by the parameter α. Although α can be treated as an adjustable parameter, for the case of hydrocarbons and fluorocarbons α is usually assumed constant and equal to 0.2, a convention that we followed for consistency with previous works.[10,49,54] Thus, only the temperature-dependent binary interaction parameters τ_{12} and τ_{21} were optimized in this work. Out of them, τ_{12}^1 and τ_{21}^1 represent the excess free energy of Gibbs divided by the ideal gas constant, while τ_{12}^0 and τ_{21}^0 lack a physical interpretation and are only used to model systems with a behavior far from ideal. Nevertheless, in the present work, the equilibria of most of the systems were accurately described using two adjustable parameters, and only the absorption of R1234yf in [C_2mim][OTf] required all four parameters due to its very low solubility. Accordingly, the NRTL model parameters, tabulated for each system in Table 8, were optimized by minimizing the average absolute relative deviation (AARD) in activity coefficients:

$$AARD = \frac{100}{N}\sum_{i=1}^{N}\frac{|\gamma_{exp} - \gamma_{calc}|}{\gamma_{exp}} \quad (18)$$

Table 8. Determined parameters for the NRTL activity-coefficient model

System	R32 + [C_2mim][BF_4]	R134a + [C_2mim][BF_4]	R134a + [C_2mim][OTf]	R1234yf + [C_2mim][OTf]	R1234yf + [C_2mim][Tf_2N]
α	0.2	0.2	0.2	0.2	0.2
τ_{12}^{0}	0	0	0	6.226	0
τ_{12}^{1}	6148.1	4794.7	5076.4	414.6	3844.6
τ_{21}^{0}	0	0	0	4.338	0
τ_{21}^{1}	51.99	278.9	99.29	-1126.1	135.2
$AARD/\%$	3.64	2.56	2.20	5.97	1.68

Interestingly, NRTL is an activity-coefficient model that has also been successfully applied to predict liquid-liquid equilibrium (LLE) of refrigerant + IL mixtures.[10] NRTL parameters presented in this work enable the prediction of immiscibility regions, defined in Figures 2-6 with dashed lines, where three phases (gas + IL with gas dissolved + liquefied gas) coexist at pressures above p_i^S.

The calculated Henry's law constants that describe the solubility behavior of the refrigerant gases at infinite dilution are presented in Table 9. As it can be seen, R32 is slightly more soluble than R134a in [C_2mim][BF_4], and R1234yf is the least soluble gas. Regarding the solubility trend for each IL, it can be observed that R134a is less soluble in [C_2mim][BF_4] than in [C_2mim][OTf], which may be related to the bigger molar volume of [C_2mim][OTf].[23,24] This hypothesis would also explain the higher solubility of R1234yf in [C_2mim][Tf_2N] than in [C_2mim][OTf]. In fact, the comparison of the Henry's law constants for R134a obtained in this work with available data, shown in Figure 7, reveals that R134a is less soluble in [C_2mim][BF_4] than in [C_2mim][OTf], and exhibits the highest solubility in [C_2mim][Tf_2N]. The same trend is also observed for R32 and R1234yf in these ILs.

Table 9. Henry's law constants (MPa) of R32, R134a and R1234yf

T/K	R32 + [C_2mim][BF_4]	R134a + [C_2mim][BF_4]	R134a + [C_2mim][OTf]	R1234yf + [C_2mim][OTf]	R1234yf + [C_2mim][Tf_2N]
283.15	1.328 ± 0.009	1.374 ± 0.010	0.811 ± 0.008	2.481 ± 0.107	1.015 ± 0.045
293.15	1.713 ± 0.005	1.996 ± 0.012	1.133 ± 0.009	3.650 ± 0.130	1.676 ± 0.048
303.15	2.297 ± 0.019	2.802 ± 0.016	1.576 ± 0.020	5.268 ± 0.091	2.378 ± 0.043
313.15	3.072 ± 0.031	3.956 ± 0.034	2.188 ± 0.017	8.203 ± 0.221	3.207 ± 0.020
323.15	3.822 ± 0.071	5.393 ± 0.059	2.759 ± 0.018	13.430 ± 0.505	4.396 ± 0.022

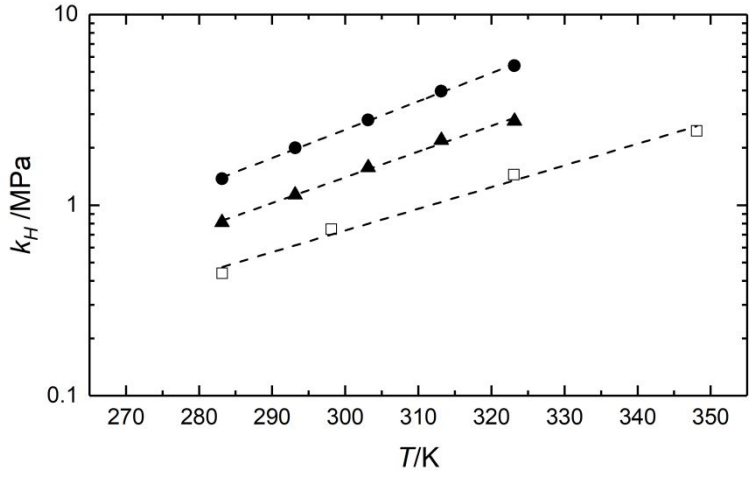

Figure 7. Henry's law constants dependence of temperature of R134a in [C_2mim][BF_4] (●), [C_2mim][OTf] (▲), and [C_2mim][Tf_2N] (■). Solid symbols represent the refrigerant-IL pairs studied in this work and hollow symbols are calculated from published data.[19] Dashed lines represent Arrhenius least-square regressions.

Eventually, the solvation enthalpy, ΔH_{sol}, and entropy, ΔS_{sol}, are calculated from Henry's law constants at infinite dilution using van't Hoff equation[55]:

$$\Delta H_{sol} = R\left(\frac{\partial \ln k_H}{\partial (1/T)}\right)_p \quad (19)$$

$$\Delta S_{sol} = -R\left(\frac{\partial \ln k_H}{\partial \ln T}\right)_p \quad (20)$$

The thermodynamic properties of solvation presented in Table 10 evidence that the absorption of refrigerants is exothermic and enthapically favorable, which can be related to the gas-IL interactions (H-bonding capability, permanent dipole moment and van der Waals forces). Yet the entropic effects are unfavorable due to the large molecule size of refrigerant gases that makes it difficult to accommodate large molecules within the IL free volume. These results are consistent with those found for similar systems in other works.[14,17]

Table 10. Thermodynamic properties of solvation

System	ΔH/(kJ·mol^{-1})	ΔS/(J·mol^{-1}·K^{-1})
R32 + [C_2mim][BF_4]	-20.479 ± 0.012	-68.4 ± 3.2
R134a + [C_2mim][BF_4]	-25.919 ± 0.003	-86.2 ± 0.9
R134a + [C_2mim][OTf]	-23.547 ± 0.006	-77.5 ± 2.8
R1234yf + [C_2mim][OTf]	-32.005 ± 0.029	-105.9 ± 7.8
R1234yf + [C_2mim][Tf_2N]	-27.011 ± 0.009	-88.1 ± 4.1

Last, solubility differences can be qualitatively explained regarding the activity coefficients at infinite dilution (γ_1^∞), which are calculated from Eq. (17) when $x_1 = 0$ and $x_2 = 1$.

$$\ln \gamma_1^\infty = \tau_{21} + \tau_{12} G_{12} \tag{21}$$

A certain compound is more soluble than ideal if $\gamma_1^\infty < 1$ and vice versa. Table 11 shows the calculated γ_1^∞ for the systems under study. As can be observed, higher values of γ_1^∞ are obtained for the least soluble pairs, and with increasing temperature.

Table 11. Fugacity coefficients at infinite dilution calculated with NRTL at various temperatures

T/K	R32 + [C_2mim][BF_4]	R134a + [C_2mim][BF_4]	R134a + [C_2mim][OTf]	R1234yf + [C_2mim][OTf]	R1234yf + [C_2mim][Tf_2N]
283.15	1.593	4.747	2.334	7.485	3.959
293.15	1.638	4.817	2.414	8.622	4.109
303.15	1.687	4.897	2.498	9.839	4.262
313.15	1.738	4.987	2.587	11.133	4.417
323.15	1.794	5.084	2.680	12.501	4.573

Regarding mass transfer rates, the diffusion coefficients at infinite dilution of R32 and R134a in [C_2mim][BF_4], R134a and R1234yf in [C_2mim][OTf] and R1234yf in [C_2mim][Tf_2N] are presented in Table 12 at temperatures between 283.15 and 323.15 K. The highest diffusion coefficients are

obtained in [C_2mim][BF_4] for the smallest molecule R32 (Chung diameter[56] is 4.02 Å). On the other hand, R134a and R1234yf have similar values of diffusion coefficient in ILs, as their molecular size is comparable (Chung diameter is 4.73 and 5.02 Å, respectively). Figure 8 shows the dependence of the diffusivity with temperature and the Arrhenius regression from which the activation energy of diffusion is calculated (Eq. (22)) and presented in Table 13:

$$D = A\exp\left(-\frac{E_D}{RT}\right) \tag{22}$$

Table 12. Binary diffusion coefficients at infinite dilution for the refrigerant-IL pairs at various temperatures

System	R32 + [C_2mim][BF_4]	R134a + [C_2mim][BF_4]	R134a + [C_2mim][OTf]	R1234yf + [C_2mim][OTf]	R1234yf + [C_2mim][Tf_2N]
T/K	$D/10^{-10}$ m^2·s^{-1}	$D/10^{-10}$ m^2·s^{-1}	$D/10^{-10}$ m^2·s^{-1}	$D/10^{-10}$ m^2·s^{-1}	$D/10^{-10}$ m^2·s^{-1}
283.15	1.67 ± 0.02	1.27 ± 0.03	1.06 ± 0.06	0.97 ± 0.06	0.36 ± 0.02
293.15	2.24 ± 0.04	1.67 ± 0.04	1.28 ± 0.02	1.26 ± 0.08	0.65 ± 0.03
303.15	3.75 ± 0.07	3.08 ± 0.06	1.85 ± 0.03	3.54 ± 0.21	1.46 ± 0.09
313.15	6.08 ± 0.10	6.40 ± 0.18	2.86 ± 0.05	4.17 ± 0.69	2.48 ± 0.31
323.15	10.04 ± 0.13	9.57 ± 0.20	5.42 ± 0.12	8.01 ± 0.88	5.14 ± 0.31

Standard uncertainty of temperature is $u(T)$ = 0.01 K. The standard uncertainties for binary diffusion coefficients at infinite dilution are given in the table.

Table 13. Arrhenius regression of diffusion coefficients for the refrigerant-IL pairs

System	A/(10^{-3} m^2·s^{-1})	E_D/(kJ·mol^{-1})	$AARD$/%
R32 + [C_2mim][BF_4]	0.28	33.9	8.01
R134a + [C_2mim][BF_4]	2.32	39.6	11.9
R134a + [C_2mim][OTf]	0.19	34.7	12.2
R1234yf + [C_2mim][OTf]	8.00	43.2	16.5
R1234yf + [C_2mim][Tf_2N]	81	50.8	6.16

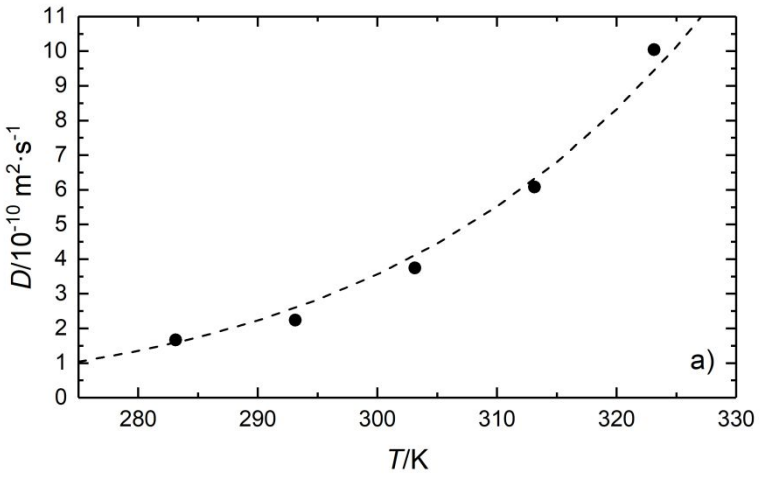

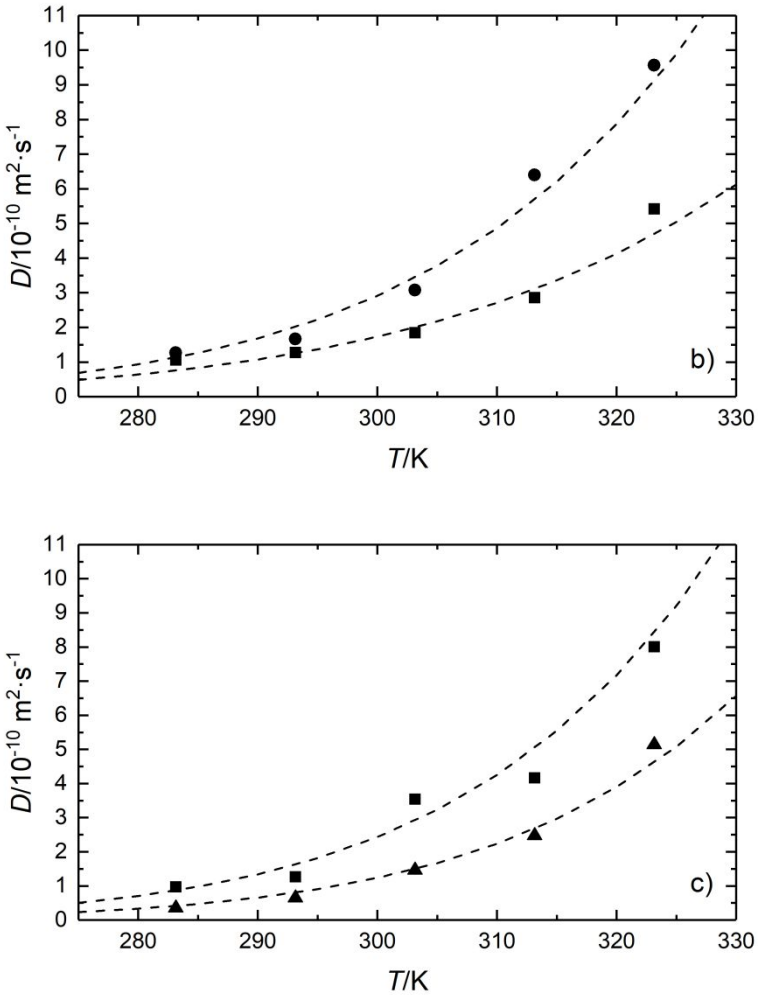

Figure 8. Diffusion coefficients dependence of temperature of a) R32, b) R134a and c) R1234yf in [C_2mim][BF_4] (●), [C_2mim][OTf] (■), and [C_2mim][Tf_2N] (▲). Dashed lines represent Arrhenius least-square regressions.

4. Conclusions

The solubility and diffusivity of HFC-32, HFC-134a, and HFO-1234yf, three important compounds present in new commercial refrigerant mixtures, was measured in the low-viscosity ILs [C_2mim][BF_4], [C_2mim][OTf] and [C_2mim][Tf_2N]. Moreover, the phase behavior of the refrigerant-IL binary systems has been successfully modeled using the NRTL activity-coefficient method with only two adjustable parameters and average deviation below 4% AARD, with the sole exception of the system R1234yf + [C_2mim][OTf], that exhibits a very low solubility and required four adjustable parameters to be accurately described (6% AARD). The Henry's law constants at

infinite dilution were calculated and used to evaluate the enthalpy and entropy of solvation, which show that the absorption of large refrigerant molecules into ILs is enthalpically favorable and exhibits unfavorable entropic contributions. In addition, the diffusion coefficients of refrigerants in ILs have been obtained using the semi-infinite volume model. As expected, the use of low-viscosity ionic liquids results in higher diffusion coefficients (10^{-10} – 10^{-9} $m^2 \cdot s^{-1}$) than those found in more viscous ILs. Overall, solubility differences observed among studied systems are significant in the field of separation, and therefore, these low-viscosity ILs could be used to separate HFCs and HFOs by means of extractive distillations with enhanced mass transfer rates.

Acknowledgements

This research is supported by Project KET4F-Gas – SOE2/P1/P0823, which is co-financed by the European Regional Development Fund within the framework of Interreg Sudoe Programme. S. A-D. and F.P acknowledge the FPU grant (18/03939) and the post-doctoral fellowship (FJCI-2017-32884 Juan de la Cierva Formación), respectively, awarded by the Spanish Ministry of Science, Innovation and Universities.

References

(1) Graziosi, F.; Arduini, J.; Furlani, F.; Giostra, U.; Cristofanelli, P.; Fang, X.; Hermanssen, O.; Lunder, C.; Maenhout, G.; O'Doherty, S.; Reimann, S.; Schmidbauer, N.; Vollmer, M. K.; Young, D.; Maione, M. European Emissions of the Powerful Greenhouse Gases Hydrofluorocarbons Inferred from Atmospheric Measurements and Their Comparison with Annual National Reports to UNFCCC. *Atmos. Environ.* 2017, *158*, 85–97.

(2) Vilaseca, O.; Llovell, F.; Yustos, J.; Marcos, R. M.; Vega, L. F. Phase Equilibria, Surface Tensions and Heat Capacities of Hydrofluorocarbons and Their Mixtures Including the Critical Region. *J. Supercrit. Fluids* 2010, *55*, 755–768.

(3) Abas, N.; Kalair, A. R.; Khan, N.; Haider, A.; Saleem, Z.; Saleem, M. S. Natural and Synthetic Refrigerants, Global Warming: A Review. *Renew. Sustain. Energy Rev.* 2018, *90*, 557–569.

(4) Nielsen, O. J.; Javadi, M. S.; Sulbaek Andersen, M. P.; Hurley, M. D.; Wallington, T. J.; Singh, R. Atmospheric Chemistry of CF3CF CH2: Kinetics and Mechanisms of Gas-Phase Reactions with Cl Atoms, OH Radicals, and O3. *Chem. Phys. Lett.* 2007, *439*, 18–22.

(5) Mota-Babiloni, A.; Makhnatch, P.; Khodabandeh, R. Recent Investigations in HFCs Substitution with Lower GWP Synthetic Alternatives: Focus on Eneretic Performance and Environmental Impact. *Int. J. Refrig.* 2017, *82*, 288–301.

(6) Mota-Babiloni, A.; Navarro-Esbrí, J.; Barragán-Cervera, Á.; Molés, F.; Peris, B. Analysis Based on EU Regulation No 517/2014 of New HFC/HFO Mixtures as Alternatives of High GWP Refrigerants in Refrigeration and HVAC Systems. *Int. J. Refrig.* 2015, *52*, 21–31.

(7) Albà, C. G.; Vega, L. F.; Llovell, F. A Consistent Thermodynamic Molecular Model of N-Hydrofluorolefins and Blends for Refrigeration Applications. *Int. J. Refrig.* 2020, *113*, 145–155.

(8) Zarca, G.; Ortiz, I.; Urtiaga, A. Recovery of Carbon Monoxide from Flue Gases by Reactive Absorption in Ionic Liquid Imidazolium Chlorocuprate(I): Mass Transfer Coefficients. *Chinese J. Chem. Eng.* 2015, *23*, 769–774.

(9) Zarca, G.; Ortiz, I.; Urtiaga, A. Kinetics of the Carbon Monoxide Reactive Uptake by an Imidazolium Chlorocuprate(I) Ionic Liquid. *Chem. Eng. J.* 2014, *252*, 298–304.

(10) Shiflett, M. B.; Yokozeki, A. Solubility and Diffusivity of Hydrofluorocarbons in Room-Temperature Ionic Liquids. *AIChE J.* 2006, *52*, 1205–1219.

(11) Asensio-Delgado, S.; Jovell, D.; Zarca, G.; Urtiaga, A.; Llovell, F. Thermodynamic and Process Modeling of the Recovery of R410A Compounds with Ionic Liquids. *Int. J. Refrig.* In press 2020.

(12) Noelke, C. J.; Shiflett, M. B. Capture of Fluorinated Vinyl Monomers Using Ionic Liquids. US Patent 8,779,220 B2, 2014.

(13) Shiflett, M. B.; Yokozeki, A. Vapor-Liquid-Liquid Equilibria of Hydrofluorocarbons + 1-Butyl-3-Methylimidazolium Hexafluorophosphate. *J. Chem. Eng. Data* 2006, *51*, 1931–1939.

(14) Shiflett, M. B.; Yokozeki, A. Gaseous Absorption of Fluoromethane, Fluoroethane, and 1,1,2,2-Tetrafluoroethane in 1-Butyl-3-Methylimidazolium Hexafluorophosphate. *Ind. Eng. Chem. Res.* 2006, *45*, 6375–6382.

(15) Shiflett, M. B.; Harmer, M. A.; Junk, C. P.; Yokozeki, A. Solubility and Diffusivity of

Difluoromethane in Room-Temperature Ionic Liquids. *J. Chem. Eng. Data* 2006, *51*, 483–495.

(16) Shiflett, M. B.; Harmer, M. A.; Junk, C. P.; Yokozeki, A. Solubility and Diffusivity of 1,1,1,2-Tetrafluoroethane in Room-Temperature Ionic Liquids. *Fluid Phase Equilib.* 2006, *242*, 220–232.

(17) Minnick, D. L.; Shiflett, M. B. Solubility and Diffusivity of Chlorodifluoromethane in Imidazolium Ionic Liquids: [Emim][Tf2N], [Bmim][BF4], [Bmim][PF6], and [Emim][TFES]. *Ind. Eng. Chem. Res.* 2019, *58*, 11072–11081.

(18) Shiflett, M. B.; Yokozeki, A. Binary Vapor–Liquid and Vapor–Liquid–Liquid Equilibria of Hydrofluorocarbons (HFC-125 and HFC-143a) and Hydrofluoroethers (HFE-125 and HFE-143a) with Ionic Liquid [Emim][Tf2N]. *J. Chem. Eng. Data* 2008, *53*, 492–497.

(19) Shiflett, M. B.; Yokozeki, A. Solubility Differences of Halocarbon Isomers in Ionic Liquid [Emim][Tf2N]. *J. Chem. Eng. Data* 2007, *52*, 2007–2015.

(20) Shiflett, M. B.; Yokozeki, A. Absorption Cycle Utilizing Ionic Liquid as Working Fluid. US Patent 8715521 B2, 2014.

(21) Shiflett, M. B. Capture of Trifluoromethane Using Ionic Liquids. US Patent Application Publication 2015/0082981 A1, 2015.

(22) Shiflett, M. B.; Yokozeki, A. Utilizing Ionic Liquids for Hydrofluorocarbon Separation. US Patent 9,628,644 B2, 2014.

(23) Lepre, L. F.; Andre, D.; Denis-Quanquin, S.; Gautier, A.; Pádua, A. A. H.; Costa Gomes, M. F. Ionic Liquids Can Enable the Recycling of Fluorinated Greenhouse Gases. *ACS Sustain. Chem. Eng.* 2019, *7*, 16900–16906.

(24) Sosa, J. E.; Ribeiro, R. P. P. L.; Castro, P. J.; Mota, J. P. B.; Araújo, J. M. M.; Pereiro, A. B. Absorption of Fluorinated Greenhouse Gases Using Fluorinated Ionic Liquids. *Ind. Eng. Chem. Res.* 2019, *58*, 20769–20778.

(25) Sun, Y.; Zhang, Y.; Wang, X.; Prausnitz, J. M.; Jin, L. Gaseous Absorption of 2,3,3,3-Tetrafluoroprop-1-Ene in Three Imidazolium-Based Ionic Liquids. *Fluid Phase Equilib.* 2017, *450*, 65–74.

(26) Zhang, Y.; Yin, J.; Wang, X. Vapor-Liquid Equilibrium of 2,3,3,3-Tetrafluoroprop-1-Ene with 1-Butyl-3-Methylimidazolium Hexafluorophosphate, 1-Hexyl-3-Methyl Imidazolium Hexafluorophosphate, and 1-Octyl-3-Methylimidazolium Hexafluorophosphate. *J. Mol. Liq*. 2018, *260*, 203–208.

(27) Liu, X.; Ye, Z.; Bai, L.; He, M. Performance Comparison of Two Absorption-Compression Hybrid Refrigeration Systems Using R1234yf/Ionic Liquid as Working Pair. *Energy Convers. Manag.* 2019, *181*, 319–330.

(28) Liu, X.; Lv, N.; Su, C.; He, M. Solubilities of R32, R245fa, R227ea and R236fa in a Phosphonium-Based Ionic Liquid. *J. Mol. Liq.* 2016, *218*, 525–530.

(29) Liu, X.; Bai, L.; Liu, S.; He, M. Vapor−Liquid Equilibrium of R1234yf/[HMIM][Tf2N] and R1234ze (E)/[HMIM][Tf2N] Working Pairs for the Absorption Refrigeration Cycle. *J. Chem. Eng. Data* 2016, *61*, 3952–3957.

(30) Liu, X.; Nguyen, M. Q.; Xue, S.; Song, C.; He, M. Vapor-Liquid Equilibria and Inter-Diffusion Coefficients for Working Pairs for Absorption Refrigeration Systems Composed of [HMIM][BF4] and Fluorinated Propanes. *Int. J. Refrig.* 2019, *104*, 34–41.

(31) He, M.; Pan, P.; Yang, F.; Wang, T.; Liu, X. Gaseous Absorption of Trans-1-Chloro-3,3,3-Trifluoropropene in Three Immidazolium-Based Ionic Liquids. *J. Chem. Eng. Data* 2018, *63*, 1780–1788.

(32) Liu, X.; Qi, X.; Lv, N.; He, M. Gaseous Absorption of Fluorinated Ethanes by Ionic Liquids. *Fluid Phase Equilib.* 2015, *405*, 1–6.

(33) Liu, X.; Pan, P.; Yang, F.; He, M. Solubilities and Diffusivities of R227ea, R236fa and R245fa in 1-Hexyl-3-Methylimidazolium Bis(Trifluoromethylsulfonyl)Imide. *J. Chem. Thermodyn.* 2018, *123*, 158–164.

(34) Dong, L.; Zheng, D.; Sun, G.; Wu, X. Vapor-Liquid Equilibrium Measurements of Difluoromethane + [Emim]OTf, Difluoromethane + [Bmim]OTf, Difluoroethane + [Emim]OTf, and Difluoroethane + [Bmim]OTf Systems. *J. Chem. Eng. Data* 2011, *56*, 3663–3668.

(35) Pardo, F.; Zarca, G.; Urtiaga, A. Separation of Refrigerant Gas Mixtures Containing R32, R134a, and R1234yf through Poly(Ether- Block -Amide) Membranes. *ACS Sustain. Chem. Eng.* 2020, *8*, 2548–2556.

(36) Zarca, G.; Ortiz, I.; Urtiaga, A. Novel Solvents Based on Thiocyanate Ionic Liquids Doped with Copper(I) with Enhanced Equilibrium Selectivity for Carbon Monoxide Separation from Light Gases. *Sep. Purif. Technol.* 2018, *196*, 47–56.

(37) Hu, X.; Meng, X.; Wu, J. Isothermal Vapor Liquid Equilibrium Measurements for Difluoromethane (R32) + Trans-1,3,3,3-Tetrafluoropropene (R1234ze(E)). *Fluid Phase Equilib.* 2017, *431*, 58–65.

(38) Dong, X.; Guo, H.; Gong, M.; Yang, Z.; Wu, J. Measurements of Isothermal (Vapour + Liquid) Equilibria Data for {1,1,2,2-Tetrafluoroethane (R134) + Trans-1,3,3,3-Tetrafluoropropene (R1234ze(E))} at T = (258.150 to 288.150) K. *J. Chem. Thermodyn.* 2013, *60*, 25–28.

(39) Kamiaka, T.; Dang, C.; Hihara, E. Vapor-Liquid Equilibrium Measurements for Binary Mixtures of R1234yf with R32, R125, and R134a. *Int. J. Refrig.* 2013, *36*, 965–971.

(40) Zarca, G.; Urtiaga, A.; Ortiz, I.; Cañizares, P.; Rodrigo, M. A. Carbon Monoxide Reactive Separation with Basic 1-Hexyl-3-Methylimidazolium Chlorocuprate (I) Ionic Liquid : Electrochemical Determination of Mass Transport Properties. *Sep. Purif. Technol.* 2015, *141*, 31–37.

(41) Palomar, J.; Larriba, M.; Lemus, J.; Moreno, D.; Santiago, R.; Moya, C.; de Riva, J.; Pedrosa, G. Demonstrating the Key Role of Kinetics over Thermodynamics in the Selection of Ionic Liquids for CO2 Physical Absorption. *Sep. Purif. Technol.* 2019, *213*, 578–586.

(42) Neves, C. M. S. S.; Kurnia, K. A.; Coutinho, J. A. P.; Marrucho, I. M.; Lopes, J. N. C.; Freire, M. G.; Rebelo, L. P. N. Systematic Study of the Thermophysical Properties of Imidazolium-Based Ionic Liquids with Cyano-Functionalized Anions. *J. Phys. Chem. B* 2013, *117*, 10271–10283.

(43) Freire, M. G.; Teles, A. R. R.; Rocha, M. A. A.; Schröder, B.; Neves, C. M. S. S.; Carvalho, P. J.; Evtuguin, D. V.; Santos, L. M. N. B. F.; Coutinho, J. A. P. Thermophysical Characterization of Ionic Liquids Able To Dissolve Biomass. *J. Chem. Eng. Data* 2011, *56*, 4813–4822.

(44) Atilhan, M.; Jacquemin, J.; Rooney, D.; Khraisheh, M.; Aparicio, S. Viscous Behavior of Imidazolium-Based Ionic Liquids. *Ind. Eng. Chem. Res.* 2013, *52*, 16774–16785.

(45) Camper, D.; Becker, C.; Koval, C.; Noble, R. Diffusion and Solubility Measurements in Room Temperature Ionic Liquids. *Ind. Eng. Chem. Res.* 2006, *45*, 445–450.

(46) Crank, J. *The Mathematics of Diffusion*, 2nd ed.; Clarendon Press: Oxford, UK, 1975.

(47) He, M.; Peng, S.; Liu, X.; Pan, P.; He, Y. Diffusion Coefficients and Henry's Constants of Hydrofluorocarbons in [HMIM][Tf2N]. [HMIM][TfO], and [HMIM][BF4]. *J. Chem. Thermodyn.* 2017, *112*, 43–51.

(48) Wentworth, W. E. Rigorous Least Squares Adjustment: Application to Some Non-Linear Equations, I. *J. Chem. Educ.* 1965, *42*, 96–103.

(49) Seader, J. D.; Henley, E. J.; Roper, D. K. *Separation Process Principles*, 3rd ed.; John Wiley & Sons, Ltd: New Jersey, USA, 2010.

(50) Bell, I. H.; Wronski, J.; Quoilin, S.; Lemort, V. Pure and Pseudo-Pure Fluid Thermophysical Property Evaluation and the Open-Source Thermophysical Property Library CoolProp. *Ind. Eng. Chem. Res.* 2014, *53*, 2498–2508.

(51) Tillner-Roth, R.; Baehr, H. D. An International Standard Formulation for the Thermodynamic Properties of 1,1,1,2-Tetrafluoroethane (HFC-134a) for Temperatures from 170 K to 455 K and Pressures up to 70 MPa. *J. Phys. Chem. Ref. Data* 1994, *23*, 657–729.

(52) Tillner-Roth, R.; Yokozeki, A. An International Standard Equation of State for Difluoromethane (R-32) for Temperatures from the Triple Point at 136.34 K to 435 K and Pressures up to 70 MPa. *J. Phys. Chem. Ref. Data* 1997, *26*, 1273–1328.

(53) Richter, M.; McLinden, M. O.; Lemmon, E. W. Thermodynamic Properties of 2,3,3,3-Tetrafluoroprop-1-Ene (R1234yf): Vapor Pressure and p - ϕ - T Measurements and an Equation of State. *J. Chem. Eng. Data* 2011, *56*, 3254–3264.

(54) Sun, Y.; Zhang, Y.; Di, G.; Wang, X.; Prausnitz, J. M.; Jin, L. Vapor-Liquid Equilibria for R1234ze(E) and Three Imidazolium-Based Ionic Liquids as Working Pairs in Absorption-Refrigeration Cycle. *J. Chem. Eng. Data* 2018, *63*, 3053–3060.

(55) Blath, J.; Christ, M.; Deubler, N.; Hirth, T.; Schiestel, T. Gas Solubilities in Room Temperature Ionic Liquids - Correlation between RTiL-Molar Mass and Henry's Law Constant. *Chem. Eng. J.* 2011, *172*, 167–176.

(56) Chung, T.-H.; Ajlan, M.; Lee, L. L.; Starling, K. E. Generalized Multiparameter Correlation for Nonpolar and Polar Fluid Transport Properties. *Ind. Eng. Chem. Res.* 1988, *27*, 671–679.

For Table of Contents use only

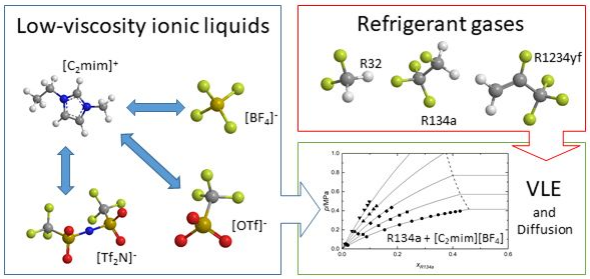

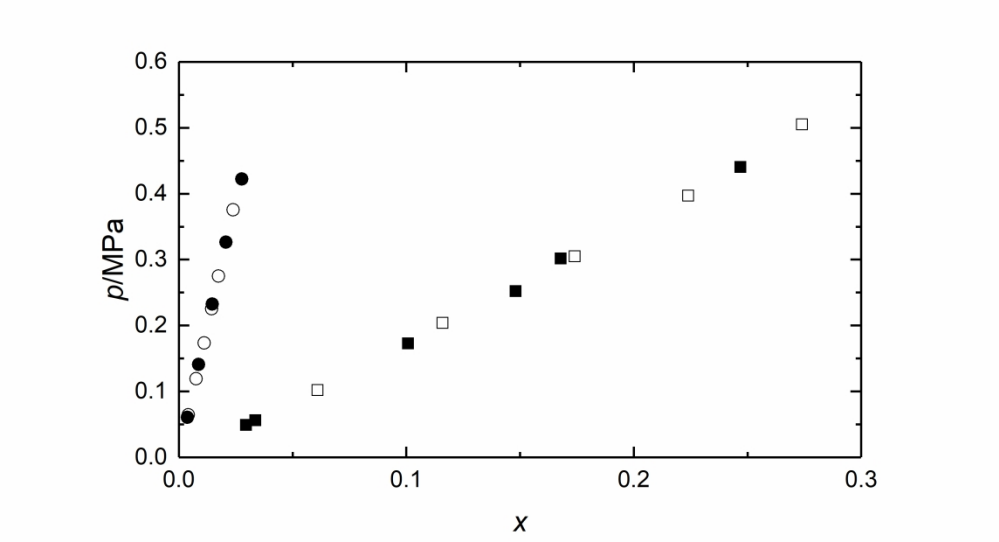

Figure 1

272x149mm (300 x 300 DPI)

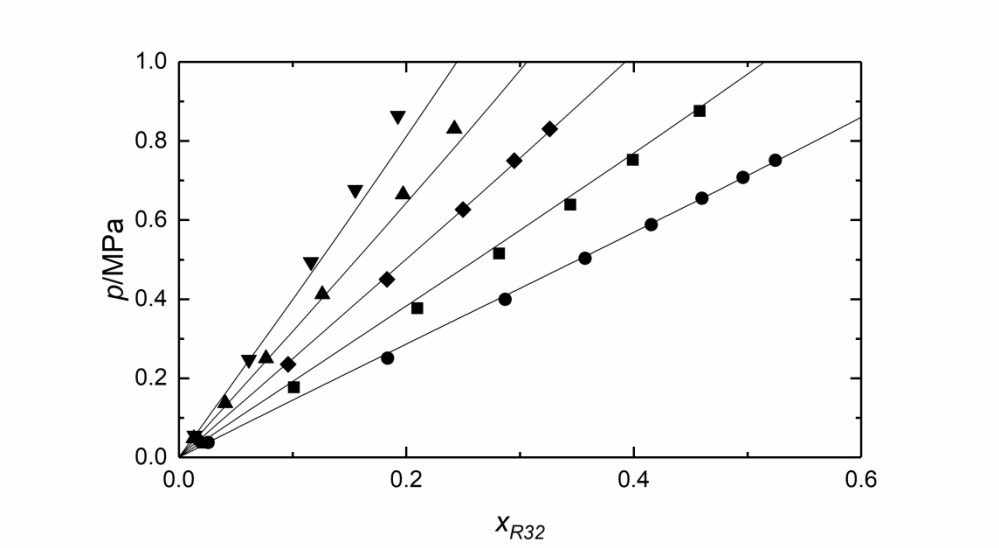

Figure 2

272x149mm (300 x 300 DPI)

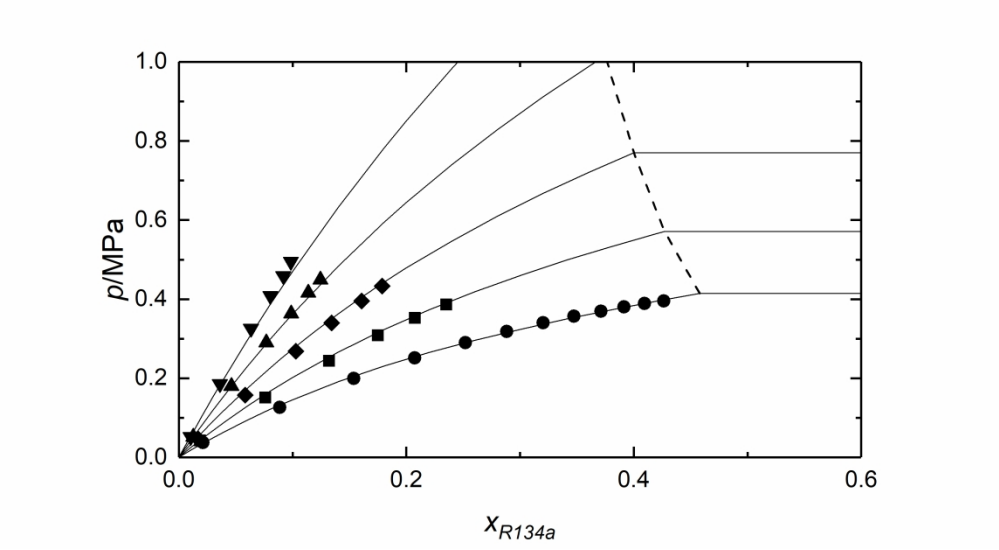

Figure 3

272x149mm (300 x 300 DPI)

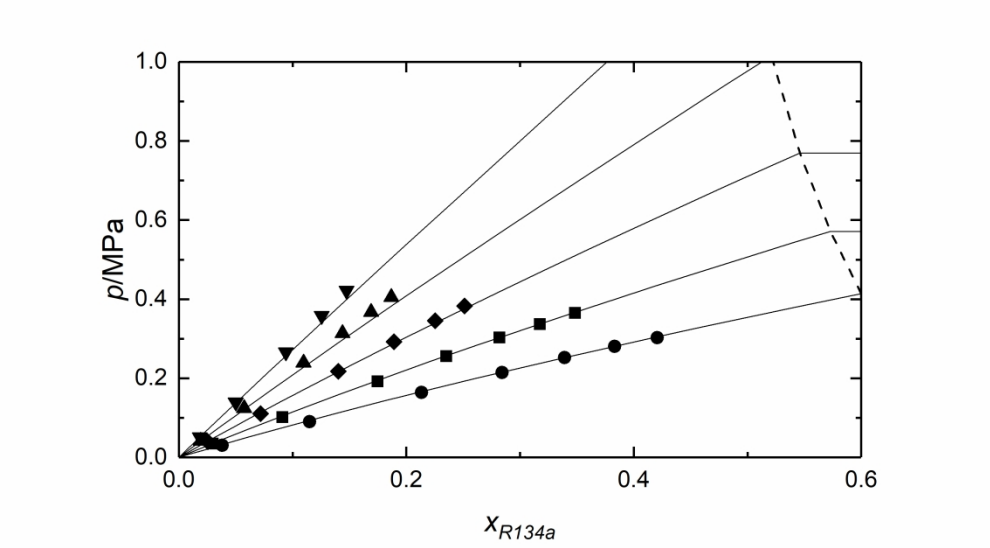

Figure 4

272x149mm (300 x 300 DPI)

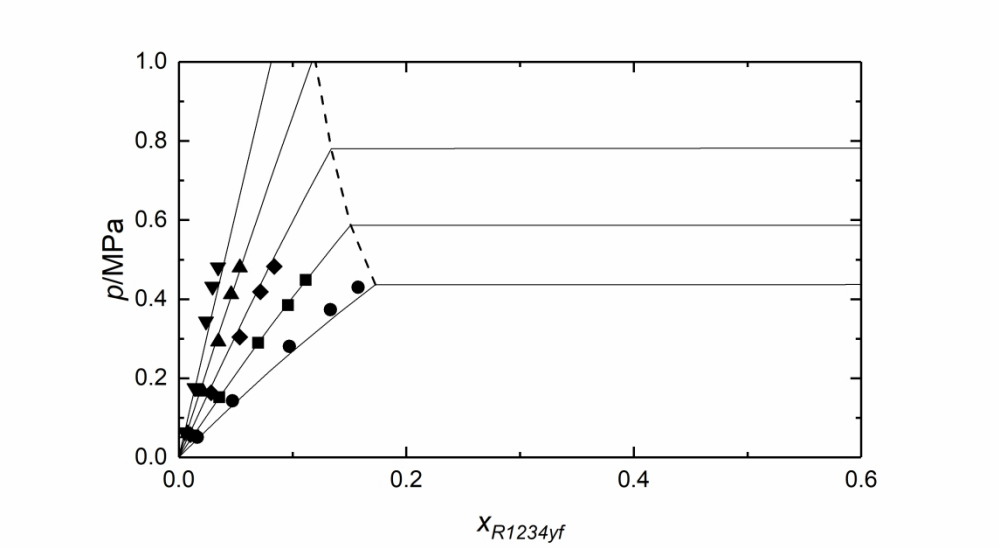

Figure 5

272x149mm (300 x 300 DPI)

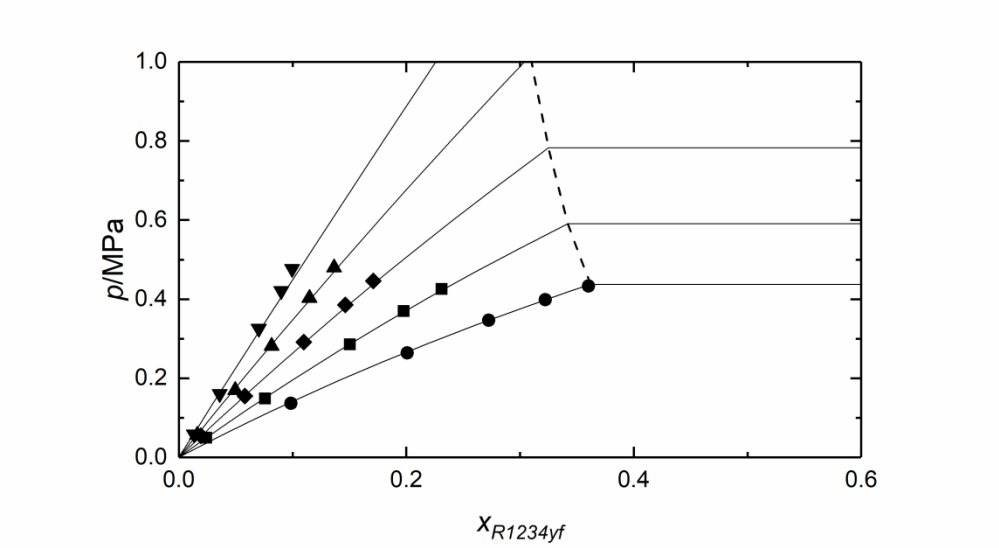

Figure 6

272x149mm (300 x 300 DPI)

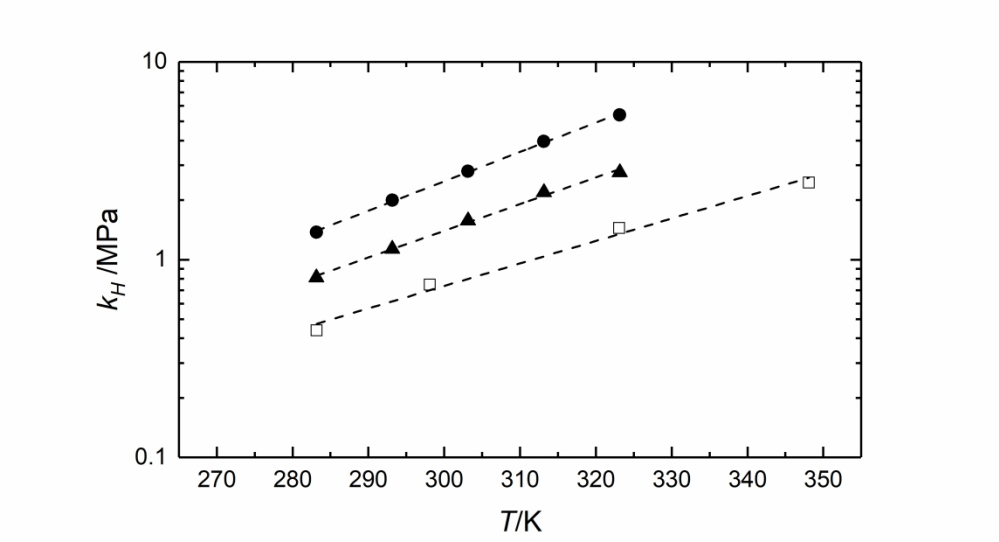

Figure 7

272x149mm (300 x 300 DPI)

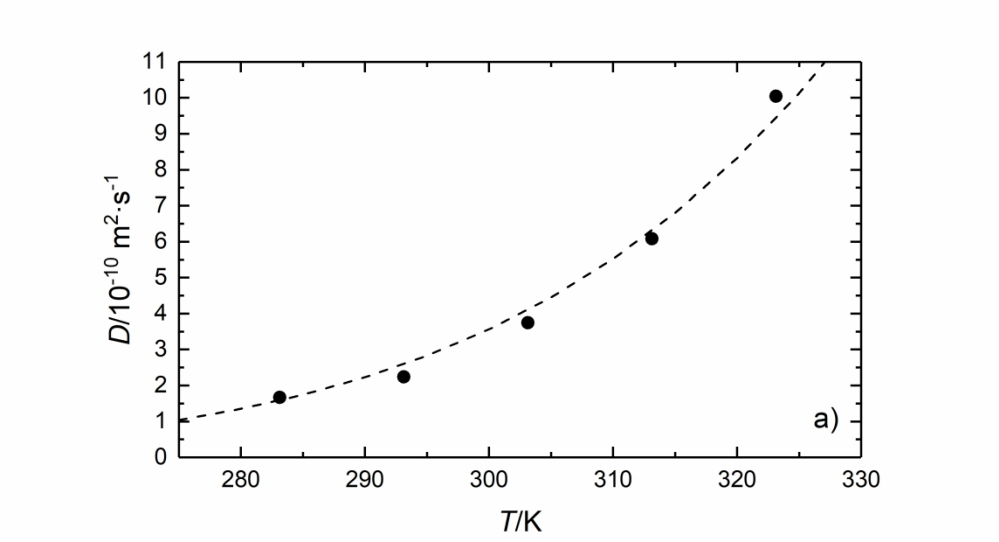

Figure 8a

272x149mm (300 x 300 DPI)

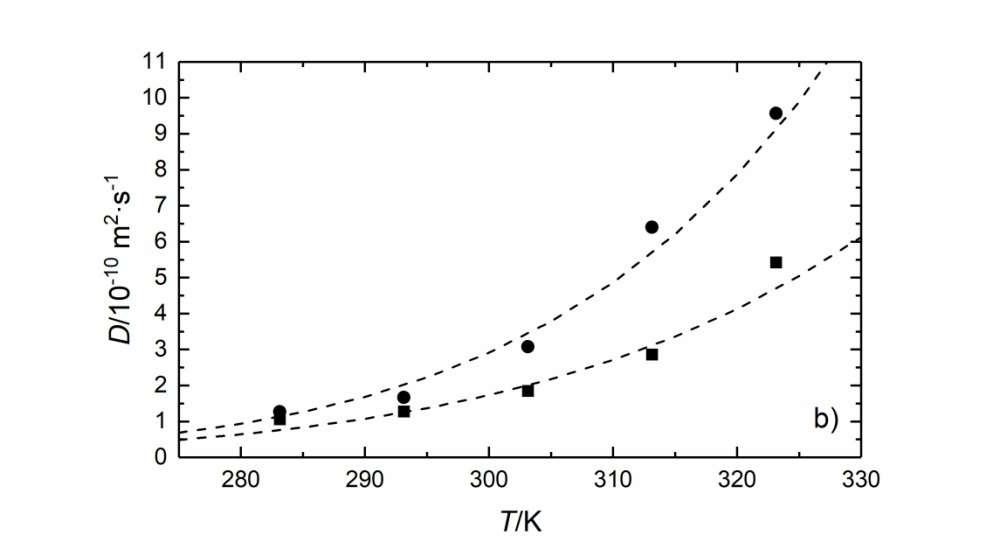

Figure 8b

272x149mm (300 x 300 DPI)

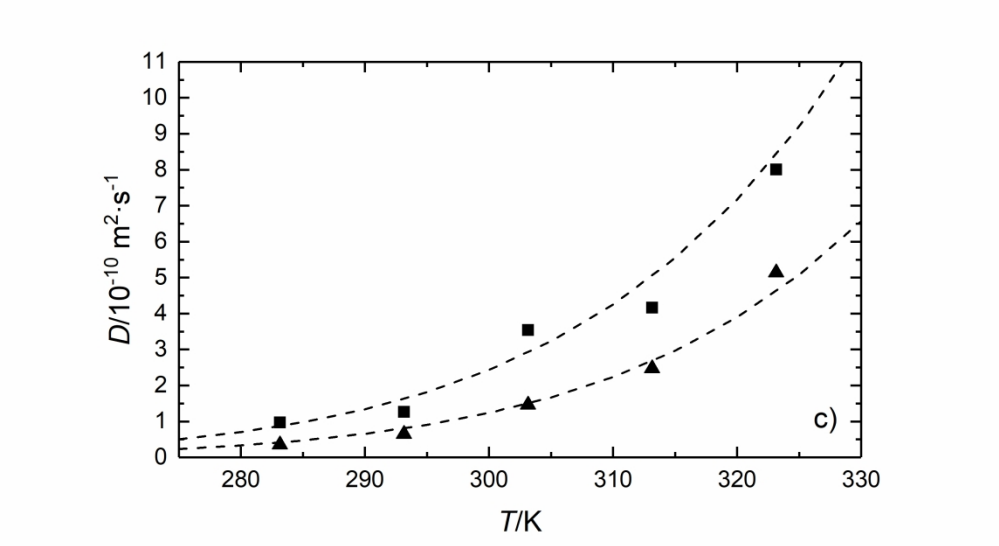

Figure 8c

272x149mm (300 x 300 DPI)

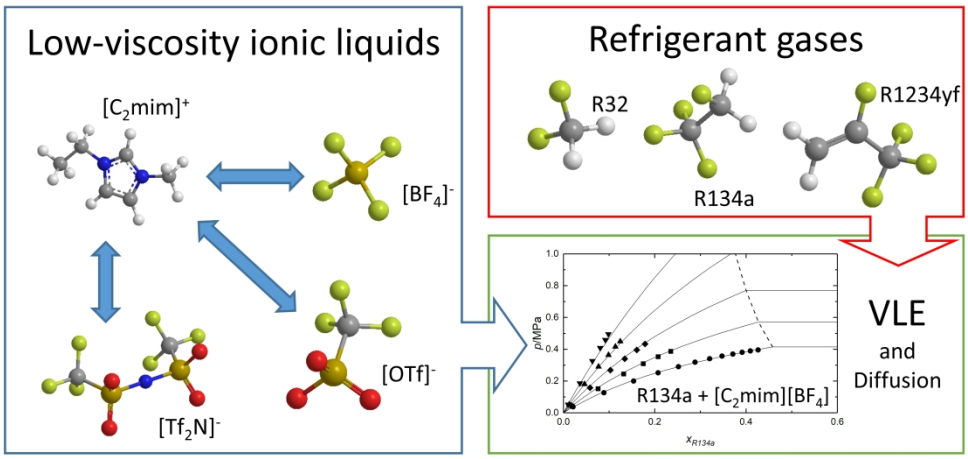

TOC graphic

159x80mm (768 x 768 DPI)